



Self-oxidation-formed boron oxide as a tunnel barrier in SmB₆ junctions

J.A. Sittler^{a,b,1}, W.K. Park^{a,*}

^a National High Magnetic Field Laboratory, Florida State University, Tallahassee, FL 32310, USA

^b Department of Physics and Astronomy, Florida State University, Tallahassee, FL 32306, USA



ARTICLE INFO

Article history:

Received 21 August 2020

Received in revised form 23 March 2021

Accepted 4 April 2021

Available online 12 April 2021

Keywords:

Boron oxide

Topological Kondo insulator

SmB₆

Correlated topological phase

Tunnel barrier

ABSTRACT

Samarium hexaboride (SmB₆) belongs to a novel class of quantum matter known as topological Kondo insulators. By utilizing planar tunneling spectroscopy, signatures of spin excitons that interact with the topological surface states have been observed. To uncover additional details about this interaction, the effect on the characteristic features by plasma cleaning and ion beam etching processes, employed to clean the SmB₆ crystal surface, are examined. Additionally, the effect of the plasma oxidation process used to form the tunnel barrier is analysed. Comparing the conductance spectra to simulations based on the Blonder-Tinkham-Klapwijk model revealed that the junctions with the highest resistances also had the weakest barrier strengths. Such seemingly contradictory observations may be explained by considering a barrier containing layers of B₆O or B₃O in addition to B₂O₃. This suboxide formation appears to be most dominant at higher ion beam energies as well as lower plasma oxidation powers.

© 2021 Elsevier B.V. All rights reserved.

1. Introduction

Samarium hexaboride (SmB₆) belongs to an interesting class of quantum matter known as topological Kondo insulators. SmB₆ is a metal at room temperature but, as the temperature is reduced, the material enters into a Kondo insulator phase [1,2] as the itinerant 5*d* bands hybridize with the localized 4*f* bands, opening up a hybridization gap. The size of this gap is generically reduced due to strong correlations. Combined with the inherently large spin-orbit coupling of the *f* electrons, this could cause the valence and conduction bands to be inverted at high-symmetry points in the momentum space [3]. If such band inversion occurs at an odd number of points, the Kondo insulator becomes topological, as predicted for SmB₆ [4]. As the chemical potential falls within the hybridization gap, the bulk of SmB₆ is insulating; yet, the surface states' bands disperse across the gap, allowing for surface conduction.

SmB₆ is close to an antiferromagnetic quantum critical point and, thus, exhibits strong magnetic fluctuations, as evidenced by the observation of spin-exciton excitations [5] as precursors to the antiferromagnetic phase transition [6,7]. These bulk spin-excitons are predicted to interact with the conducting surface states [7] and

signatures of this interaction have been observed in previous experiments using planar tunneling spectroscopy (PTS) [8–10].

Analogous to a procedure developed by McMillan and Rowell [11], information in the second harmonic spectra of SmB₆ tunnel junctions may help reveal the spectral density of the spin excitons and the strength or energy dependence of their interaction with the conducting surface states. As the second harmonic signal is generically weak, it is easily overwhelmed by noises. For this reason, it is paramount that the junctions fabricated are of the highest quality possible.

PTS is ideally suited for the study of surface states owing to its inherent surface-sensitiveness as well as high energy resolution and momentum selectivity [12]. A tunnel junction is comprised of a bottom electrode, typically the material of interest, an insulating barrier, and a counter-electrode, as shown in the inset of Fig. 1(a). The differential conductance, $(V) \equiv dI/dV$, for tunneling between a material whose density of states (DOS) is a constant near its Fermi energy, $d_c(0)$, and the material of interest, $d_s(E)$, is given by the convolution of $d_s(E)$ with respect to the derivative of the Fermi function:

$$\frac{dI}{dV} = A |T|^2 d_c(0) e^2 \int_{-\infty}^{\infty} d_s(E) \frac{\partial f(E - eV)}{\partial (eV)} dE, \quad (1)$$

where A is the junction area and T is the tunneling matrix element. In this work, Pb is utilized as the top electrode as the sharpness of its superconducting features is ideal for junction quality diagnostics

* Corresponding author.

E-mail address: wkpark@magnet.fsu.edu (W.K. Park).

¹ Present address: Department of Physics, University of California Santa Cruz, Santa Cruz, CA 95064, USA.

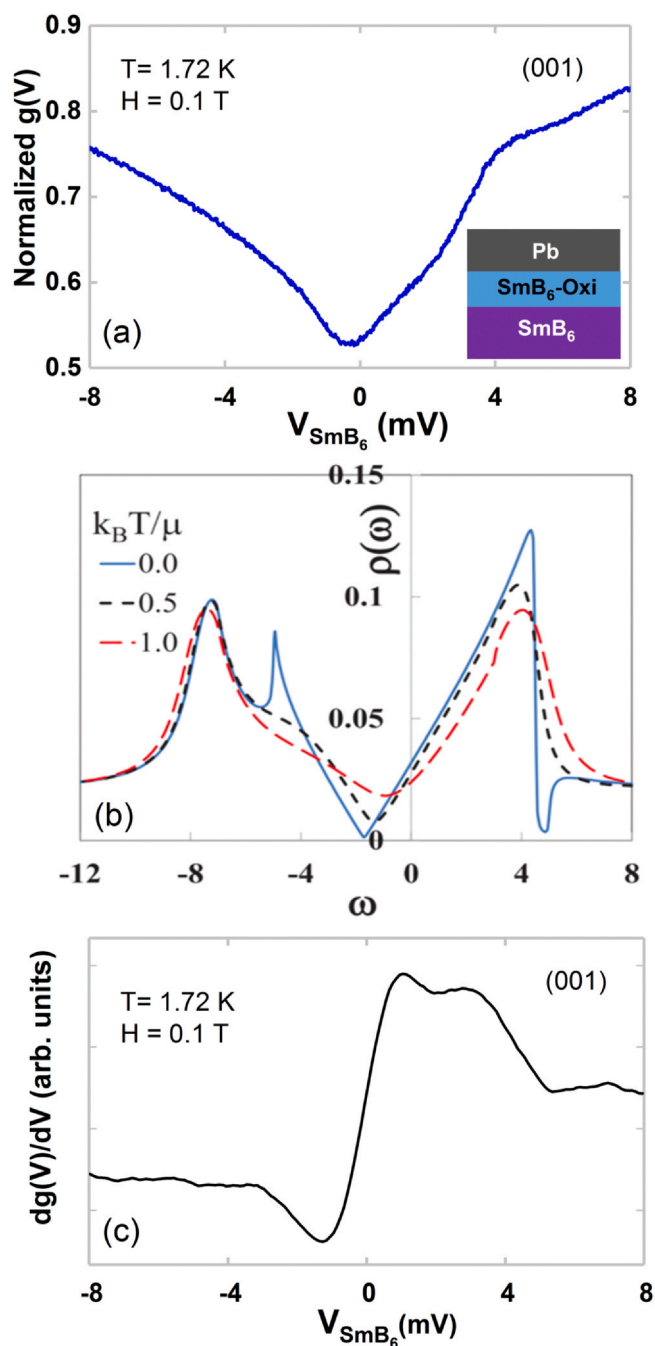


Fig. 1. (a) Influence of spin excitons on the conducting surface states. (a) $g(V)$ of a $\text{SmB}_6/\text{SmB}_6\text{-Oxi}/\text{Pb}$ junction at $H = 0.1$ T. Inset: side view of a $\text{SmB}_6/\text{SmB}_6\text{-Oxi}/\text{Pb}$ junction. (b) Theoretically predicted spectral density of SmB_6 . Plots (a) and (b) are V-shaped at low bias due to the conducting surface states and show a disruption at ± 4 mV likely due to the surface states interaction with the bulk spin excitons. (c) Second derivative curve of a high quality $\text{SmB}_6/\text{SmB}_6\text{-Oxi}/\text{Pb}$ junction found from numerically differentiating the $g(V)$ curve. The two positive bias peaks around 1 mV and 2.5 mV are likely due to the two distinct slopes in plot (a) which correspond to the two Dirac cones observed for the (001) surface orientation [8]. (a) Adapted from Ref. [8]. (b) Adapted from Ref. [7]

and allows for comparison to the Blonder-Tinkham-Klapwijk (BTK) model [13]. Additionally, by applying a magnetic field driving the Pb normal, the DOS of the conducting surface states of SmB_6 is revealed.

A variety of methods have been tried to create a tunnel barrier on SmB_6 crystals including depositing a layer of Al and then oxidizing it [9]. However, due to inter-diffusion between the deposited Al layer and the SmB_6 crystal, such attempts were unsuccessful. Thus far, the

method that is able to reproducibly create the highest-quality junctions is self-oxidation of the SmB_6 crystals ($\text{SmB}_6\text{-Oxi}$) using an oxygen plasma [8,9]. Other work has also reported results from SmB_6 junctions with a self-oxide barrier formed by thermal oxidation [14]. However, detailed conductance features as seen in the plasma-oxidized junctions [8] are missing. The conductance spectra of our junctions (Fig. 1(a)) are consistent with the theoretically predicted DOS of SmB_6 (Fig. 1(b)). At low bias voltages, both graphs show the characteristic V-shape due to the conducting surface states and show a disruption in this V-shape at ± 4 mV, likely due to the surface states' interaction with the bulk spin excitons [8,10]. These detailed features seen in our PTS have not been observed in scanning tunneling [15–17] and point-contact [18] spectroscopic measurements. In particular, the conductance curves obtained with scanning tunneling microscopes largely resemble the Fano lineshape arising from tunneling into a local single Kondo impurity. It remains to be investigated whether/how the desired global spectroscopic information can still be extracted from such local tunneling spectra.

A second derivative curve obtained by numerically differentiating the first harmonic data of a $\text{SmB}_6/\text{SmB}_6\text{-Oxi}/\text{Pb}$ junction at $H = 0.1$ T is shown in Fig. 1(c), where a large structure is observed in the low positive-bias region which could possibly be due to the spin excitons. Additionally, this curve shows two positive bias peaks around 1 mV and 2.5 mV, likely due to the two distinct slopes shown in Fig. 1(a) corresponding to the two Dirac cones observed for the (001) surface orientation [8]. To obtain detailed features that cannot be resolved from the mathematically differentiated curve, the second harmonic must be measured directly from high-quality junctions.

In this work, we investigate the effects of two different methods of surface cleaning: plasma cleaning and ion beam etching. For the junctions fabricated on top of the plasma-cleaned SmB_6 surfaces, the effect of the plasma oxidation conditions used to create the insulating barrier is investigated. Junctions processed with either cleaning method showed the expected V-shaped conductance and spin exciton features. In addition, the junctions processed with a higher plasma oxidation power ($P_{\text{pl-oxi}}$) showed the highest quality features.

2. Experiment

2.1. SmB_6 junction fabrication procedure

The SmB_6 junctions are created on SmB_6 crystals grown by both flux [19] and floating zone [20] methods. The junction fabrication procedure is described in detail elsewhere [8,9] and schematically depicted in Fig. 2. As the crystals are relatively small having a thickness of ~ 0.5 mm and a length of 1–2 mm, they are embedded into an epoxy (Stycast®) mold for increased functionality. The crystals are polished to sub-nanometer roughness, as verified by the topographic profile obtained with an atomic force microscope, by mechanically rubbing them against alumina lapping films ranging in particle size from 12 to 0.3 μm . Then the crystal surface is cleaned with either an argon ion beam or an *rf* argon plasma in different vacuum chambers. The tunnel barrier is formed by exposing the crystal surface to an oxygen plasma in the same system as used for the surface cleaning generated by *dc* glow discharge and *rf* source, respectively. During the oxidation process, the surface states of SmB_6 reform underneath the newly-formed insulating layer [8], where they are protected from any disorder such as surface reconstruction [17].

After the sample is taken out of the chamber, it is painted with acetone-diluted Duco® cement to define the junction area and to cover any rough edges that may be present on the sides of the crystal. The Pb electrode is then deposited through a shadow mask in a thermal evaporator. A moderate deposition rate of 8–10 $\text{\AA}/\text{s}$ is

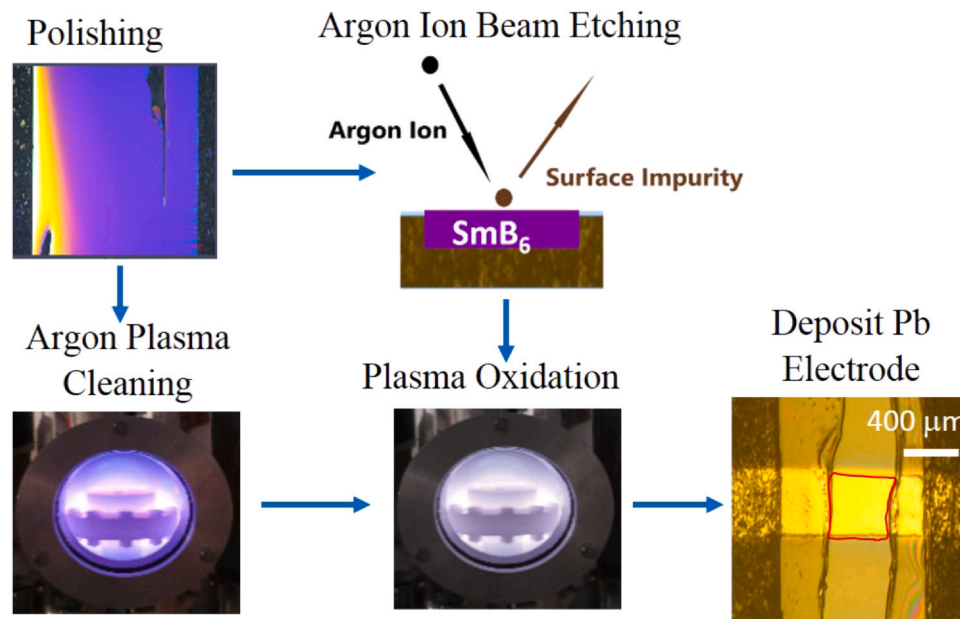


Fig. 2. Schematic of the fabrication processes of a $\text{SmB}_6/\text{SmB}_6\text{-Oxi}/\text{Pb}$ tunnel junction. The SmB_6 crystal is first polished to sub-nanometer roughness and the surface of SmB_6 is then cleaned with either an argon ion beam (ion beam etching) or with an argon plasma (plasma cleaning). The insulating barrier is then formed by plasma oxidizing the top layer of the SmB_6 crystal. Lastly, the sides of the crystal are painted and a Pb electrode is deposited through a shadow mask using a thermal evaporator. The junction area is outlined with a red square in the bottom right image.

used to prevent damages to the tunnel barrier and the thickness of the Pb layer is $\cong 2500 \text{ \AA}$.

2.2. Surface cleaning

Both plasma cleaning and ion beam etching are able to remove surface-oxides or residual contaminants. However, ion beam etching is a harsher process than plasma cleaning and, thus, is more likely to knock off atoms in SmB_6 since the argon ions are accelerated toward the crystal. Additionally, Sm has a much higher sputter yield than B (e.g., 2.13 vs. 0.31 for 500 eV of beam energy [21]), so the surface layer is likely to consist of B atoms rather than Sm atoms after the ion beam etching process. This is consistent with the tunnel barrier formed by the optimized plasma oxidation being B_2O_3 , as confirmed by x-ray photoemission spectroscopy (XPS) [9].

2.3. Junction measurement

After the junction is fabricated, wires are attached to the sample using silver paint. The sample is then placed into a Quantum Design Physical Property Measurement System[®], where it is cooled down to 1.75 K. Four-probe conductance measurements are carried out using a custom mixing circuit and LabVIEW is used to collect the data. The differential quantities in current (dI) and voltage (dV) are measured at a fixed frequency (633 Hz) using separate lock-in amplifiers, allowing for the differential conductance to be measured directly.

2.4. Junction characterization

Regardless of junction type, the main contributors to the junction quality are the tunnel barrier and its interface with the bottom and top electrodes. As shown in Fig. 3, for a high quality junction, the electrostatic potential of the insulating barrier should be high enough compared to the maximum bias voltage and the two interfaces should be sharp [8,9]. Additionally, the ratio of $g(V)$ at zero bias to $g(V)$ at the edge of the superconducting gap should be low and the junction should show clean conductance spectra resembling the DOS of the superconductor (Pb).

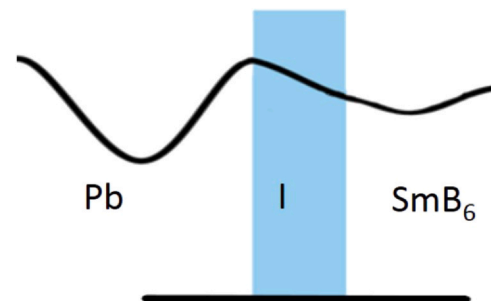


Fig. 3. Cartoon of quantum tunneling. The Pb electrode and SmB_6 electrode are separated by an insulating barrier I. For high quality junctions, the electrostatic potential of the insulating barrier should be high compared to the maximum bias voltage. Additionally, the barrier should be uniform over the entire junction area, sharp at both interfaces, and free of any impurities that may cause scattering.

In Fig. 4, the differential conductance of a high-quality junction that was fabricated on a surface processed with an ion beam energy (E_B) of 100 eV is plotted alongside a best-fit curve to the Brinkman-Dynes-Rowell (BDR) model for a tunnel barrier [22]. As the thickness and mean barrier height affect the symmetrical and asymmetrical conductance terms differently, numerical values may be obtained from this model. We obtain the thickness of the barrier $\cong 10.0 \text{ \AA}$, the potential barrier height $\cong 11.9 \text{ eV}$, and the asymmetry = 0.8 eV, which are indicative of a high-quality tunnel barrier.

For high-quality SmB_6 junctions, the conductance spectra at low-temperature are expected to reveal asymmetric coherence peaks as well as an additional peak at $\sim 5 \text{ mV}$. In previous experiments, these features were attributed to inelastic tunneling processes involving the spin excitons [8–10].

3. Results

No noticeable differences in the formation of the tunnel barrier have been observed from the crystals grown with flux [19] or floating zone [20] methods despite the known Sm deficiency in the latter (up to 1%). This is very much expected since the

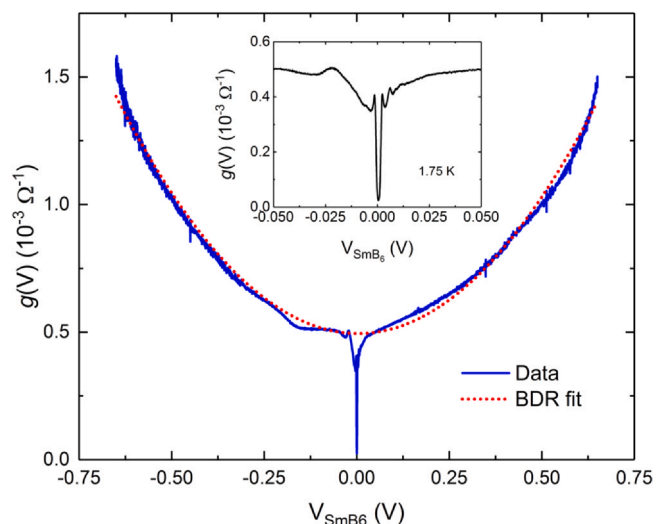


Fig. 4. Analysis of the barrier characteristics in a high-quality $\text{SmB}_6/\text{SmB}_6\text{-Oxi}/\text{Pb}$ junction. Tunneling conductance taken at 1.75 K of a high-quality $\text{SmB}_6/\text{SmB}_6\text{-Oxi}/\text{Pb}$ junction (blue solid line) and the best-fit curve to the Brinkman-Dynes-Rowell (BDR) model (red dotted line) [16]. The junction was formed on an ion-beam-etched surface. The BDR model was fit to the parabolic background and the extracted barrier parameters are: the thickness $\cong 10.0 \text{ \AA}$, the potential barrier height $\cong 11.9 \text{ eV}$, and the asymmetry = 0.8 eV, indicative of a high-quality tunnel barrier. This is also evidenced by the inset where the same conductance is zoomed at low bias. All features characteristic of a high-quality tunnel junction are observed including the broad peak around -21 mV , the asymmetric Pb coherence peaks, and the extra peak around 5 mV arising from inelastic tunneling involving spin excitons [8].

plasma-oxidized B_2O_3 is the acting tunnel barrier. In other words, our findings reported here are independent of the crystals, so the crystal types are not distinguished in this paper. The detailed conductance features do show intriguing discrepancies between stoichiometric and Sm-deficient crystals, as reported elsewhere [10].

3.1. SmB_6 surface prepared with ion beam etching

As mentioned in Section 1, by applying a magnetic field above the critical field, the Pb electrode will become flat in its DOS near its

Fermi level, and the conductance spectra of a high-quality junction will resemble the DOS of the conducting surface states in SmB_6 as shown in Fig. 5(a), which is not flat unlike a simple metal. The contribution from the background of SmB_6 can be canceled by dividing out the conductance taken at zero field by the one taken at $H = 0.1 \text{ T}$. The resulting normalized conductance is expected to resemble the DOS of Pb. However, additional features arising from inelastic tunneling involving spin exciton excitations are observed [8], as shown in Fig. 5(b).

When the Pb electrode is driven normal (Fig. 5(a)), the characteristic V-shaped conductance is not present for the crystal cleaned with $E_B = 200 \text{ eV}$. With $E_B = 100 \text{ eV}$, the V-shaped conductance as well as the kinks at $\pm 5 \text{ mV}$ likely due to the spin excitons are observed. On the contrary, with $E_B = 50 \text{ eV}$ the V-shaped conductance is observed but the spin exciton features are not. As shown in Fig. 5(b), the junctions processed with $E_B = 50 \text{ eV}$ or 200 eV did not show clear inelastic tunneling features as no additional conductance peak at around 5 mV is observed. This additional peak is clearly seen for the high-quality junction produced with $E_B = 100 \text{ eV}$.

By normalizing $g(V)$ with the Pb superconducting against $g(V)$ normal, the normalized $g(V)$ may be approximated using the BTK model [13]. The BTK fitting was done using a code that automatically finds the best fit to the data by varying fit parameters such as the superconducting gap (Δ), smearing factor (Γ), and dimensionless barrier strength (Z). Although all three parameters are interconnected to fit the data, the code works by changing the parameters based on their dominant effect and then making small corrections based on their recessive effects. The dominant effect of Z is to lower the zero-bias conductance. The dominant effect of Γ is to decrease the peak height and the dominant effect of Δ is to increase the peak-to-peak distance. We note that the adopted BTK model [13] is based on simple possible transport processes across a normal-metal/insulator/superconductor junction, namely, single Andreev reflection and single-step elastic tunneling. As discussed later, other transport processes such as hopping and diffusion may also contribute to the conductance in some low-quality junctions. In such cases, the extracted Z values need to be interpreted with this aspect taken into account.

The best fit curves are shown along with the data in Fig. 6 and the different parameters used for the BTK simulations are listed in

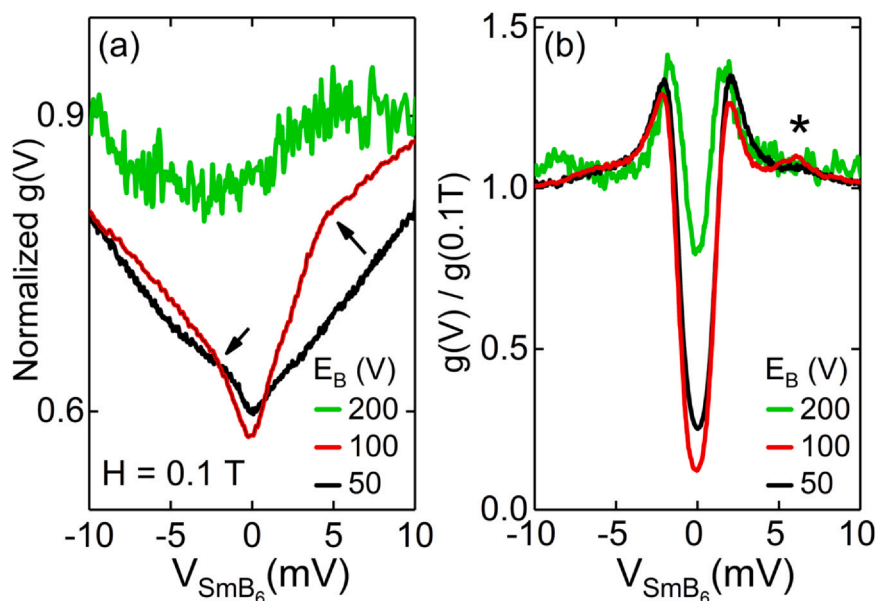


Fig. 5. Conductance spectra of $\text{SmB}_6/\text{SmB}_6\text{-Oxi}/\text{Pb}$ junctions processed with ion beam etching. The arrows and asterisk mark spin exciton features. (a) The Pb electrode is driven normal by magnetic field ($H = 0.1 \text{ T}$). (b) The $g(V)$ curves at zero field divided by the $g(V)$ curves at $H = 0.1 \text{ T}$. Overall, the junctions produced with the lower ion beam energies (E_B) are the highest quality and the spin exciton features are most clearly seen in the junction produced with $E_B = 100 \text{ eV}$.

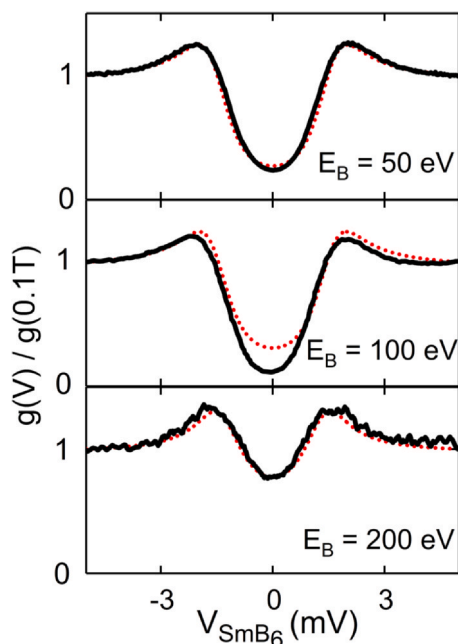


Fig. 6. Background-normalized conductance spectra of SmB₆/SmB₆-Oxi/Pb junctions processed with ion beam etching and the best fits to the BTK model. $g(V)$ curves for SmB₆/SmB₆-Oxi/Pb junctions at zero field divided by $g(V)$ at $H=0.1$ T (black solid lines) and the best fits to the BTK model [12] (red dotted lines). The ion beam energy (E_B) used for each junction is as indicated.

Table 1

Characteristics of the junctions prepared with ion beam etching and best-fit parameters for the BTK analysis.

E_B (eV)	50	100	200
R_j at 1.8 K (Ω)	31	2083	3900
A_j (mm ²)	0.18	NA	NA
Δ (meV)	1.50	1.55	1.45
Z	10.0	10.0	0.8
Γ (meV)	0.37	0.40	0.30

From top to bottom, the table lists the ion beam etching energy (E_B) used to clean the SmB₆ surface, the junction parameters such as the resistance at 1.8 K (R_j) and the junction area (A_j) as well as the parameters used for the BTK fits, such as the superconducting gap (Δ), the barrier strength (Z), and the smearing parameter (Γ). With increase in E_B , the resistance increases, yet a large drop in Z is observed when $E_B = 200$ eV. This observation is contradictory to the resistance and barrier strength relation the BTK theory proposes [12].

Table 1. Notice how the junction resistance (R_j) increases with E_B yet the Z value drops to 0.8 when $E_B = 200$ eV.

3.2. SmB₆ surface prepared with plasma cleaning

The conductance spectra of junctions prepared with the plasma cleaning step are shown Fig. 7. Fig. 7(a) shows the conductance spectra when the Pb electrode is driven normal by applied magnetic field ($H = 0.1$ T) and Fig. 7(b) shows the differential conductance at zero magnetic field divided by the differential conductance at $H = 0.1$ T. The conditions under which each junction was prepared are listed in Table 2. The junctions are labeled and ordered alphabetically, firstly, by the $P_{\text{pl-oxi}}$ and secondly by the duration of plasma oxidation ($t_{\text{pl-oxi}}$) or duration of plasma cleaning (t_{clean}). For example, a junction prepared with $P_{\text{pl-oxi}} = 3$ W and $t_{\text{pl-oxi}} = 10$ s would be listed before a junction prepared with $P_{\text{pl-oxi}} = 3$ W and $t_{\text{pl-oxi}} = 30$ s. All junctions were processed with the same plasma cleaning power of 30 W.

In Fig. 7(a), all junctions, except junction C which did not undergo any surface cleaning, exhibit V-shaped conductance at low bias. Additionally, junction E shows a kink at around +4 mV and a hump

at around -2 mV, which are similar to the expected features of spin excitons discussed earlier. Junction D also shows hints of the spin excitons as there is a change in the linearity, but the features are quite smeared.

Junction E, the junction processed with the highest $P_{\text{pl-oxi}}$, shows the highest quality features in Fig. 7(b) as well. This junction clearly shows an additional peak at around 5 mV and asymmetrical coherence peaks. On the other hand, junction C shows the lowest quality features, suggesting the importance of surface cleaning as junction D was processed with the same oxidation conditions yet shows relatively high-quality features.

To investigate how the different process conditions affect the parameters, Γ , Z and Δ , the data were fit to the BTK model. The best fit curves are shown in Fig. 8 and the parameters used to fit the data are shown in Table 2. Although the fit for junction C (Fig. 8) shows large deviations from the data, the larger Z value is justified given that the zero-bias conductance is so low, and the high smearing is justified given that there were no coherence peaks seen. From Table 2, notice that when the $P_{\text{pl-oxi}}$ is decreased R_j increases and Z decreases. This relation between R_j and Z is a seemingly contradictory behavior, yet it is also observed for the ion beam etched junctions.

4. Discussion

Junction cleaning is shown to be a crucial step in the junction fabrication process. In ion beam etching, E_B greatly influenced the quality of the features seen. Moreover, plasma cleaning greatly improved the junction quality as well. Compared to junction C, which did not undergo any surface cleaning, the junctions that were plasma cleaned showed significantly less smearing, and the features seen were of higher quality overall. Additionally, Junction E, produced with the longest duration of plasma cleaning, produced the highest quality features.

For the ion beam etched junctions, the junction cleaned with $E_B = 100$ eV displayed the highest quality features as all the expected spin exciton features were seen (Fig. 5). Nonetheless, this junction has a significant smearing factor ($\Gamma = 0.40$ meV) which could conceal features that would otherwise be detectable in the second harmonic.

Unlike the junctions processed with $E_B = 50$ eV and 100 eV, the junction processed with $E_B = 200$ eV did not show V-shaped conductance at low bias. Additionally, this junction displayed the highest R_j yet the lowest Z value; a relationship contradictory to the BTK theory which defines R_j as depending quadratically on Z [13]. The low-quality junctions prepared on the plasma cleaned SmB₆ crystals, namely junction A and B, also possessed the highest R_j yet the lowest Z values.

For high quality junctions, the insulating barrier is most likely composed of B₂O₃ as suggested by band structure calculations showing that B₂O₃ has a large band gap (6–9 eV) [23], which is consistent with the high Z values observed. The calculated band gap of B₂O₃ is slightly lower but still in rough agreement with the potential barrier height ($\cong 12$ eV) estimated for a high-quality junction in Section 2.4. Conversely, to explain the high R_j and low Z values observed for the low quality junctions, it is worth considering an insulating barrier primarily composed of suboxides, as electrons tunneling through different oxide layers would undergo a more complicated diffusion/tunneling process. Additionally, previous studies utilizing XPS observed the development of B₆O and B₃O to form in layers underneath B₂O₃ [24]. The presence of these semi-conducting suboxides [25] would be able to explain the low Z values, as semiconductors have a smaller band gap. Additionally, these suboxides may penetrate deep into the sample, explaining the higher R_j observed.

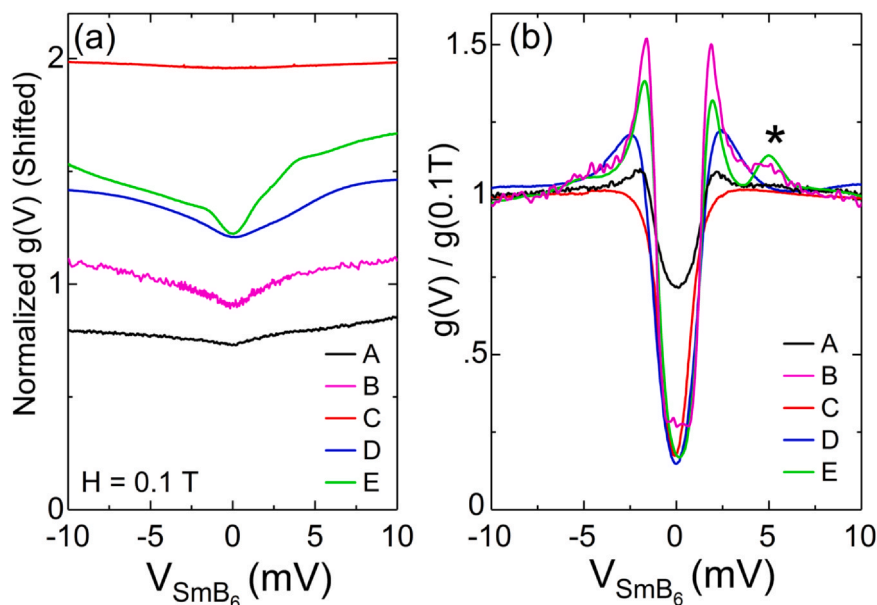


Fig. 7. Conductance spectra of $\text{SmB}_6/\text{SmB}_6\text{-Oxi}/\text{Pb}$ junctions processed with plasma cleaning. (a) The Pb electrode is driven normal by magnetic field ($H = 0.1$ T). Junction E and D produced with the highest power of oxidation, appear to be the highest quality as they show a kink at $+4$ mV or a hump at -2 mV likely due to spin excitons. (b) The $g(V)$ curve for Pb in the superconducting state normalized against the $g(V)$ curve for Pb in the normal state. The asterisk marks a feature likely due to the emission of spin excitons and is the most pronounced in junction E.

Table 2

Processing parameters for the junctions prepared with plasma cleaning, their characteristics and best-fit parameters for the BTK analysis.

Junction	A	B	C	D	E
t_{clean} (s)	60	60	NA	60	120
$P_{\text{pl-oxi}}$ (W)	3	3	5	5	10
$t_{\text{pl-oxi}}$ (s)	10	30	60	60	60
R_j at 1.75 K (Ω)	1126	9300	374	373	485
A_j (mm^2)	0.68	NA	NA	NA	NA
Δ (meV)	1.725	1.66	2.5	1.65	1.325
Z	1.154	1.69	10	10	10
Γ (meV)	0.891	0.177	0.946	0.451	0.225

From top to bottom, the table lists the duration of the plasma cleaning (t_{clean}), the power of the plasma oxidation ($P_{\text{pl-oxi}}$), and the duration of plasma oxidation ($t_{\text{pl-oxi}}$). This is followed by the junction parameters such as the junction resistance at 1.8 K (R_j) and the junction area (A_j) as well as the parameters used for the BTK fits, such as the superconducting gap (Δ), the barrier strength (Z), and the smearing parameter (Γ). Comparing junctions A and B, fabricated with $P_{\text{pl-oxi}} = 3$ W, an increase in $t_{\text{pl-oxi}}$ results in a large increase in R_j . However, when $P_{\text{pl-oxi}}$ is increased to 5 W, and $t_{\text{pl-oxi}}$ is increased to 60 s, a decrease in R_j is observed. Similar to the junctions fabricated with ion beam etching, the junction with higher R_j also displayed lower Z values which is contradictory to the relation the BTK theory proposes [12].

For the junctions prepared on the plasma cleaned SmB_6 surfaces, junction A and B, prepared with the lowest plasma oxidation power, $P_{\text{pl-oxi}}$, displayed the highest R_j and lowest Z values, possibly due to the formation of suboxides. Conversely, junction C, D and E processed with the highest $P_{\text{pl-oxi}}$ showed the lowest R_j and highest Z values. Notice that a larger $t_{\text{pl-oxi}}$ and $P_{\text{pl-oxi}}$ were used in the fabrication of junctions C, D, and E than for junctions A and B. However, the improvement in the Z and R_j values observed for C, D, and E can be attributed to the increase in $P_{\text{pl-oxi}}$ as changes in $t_{\text{pl-oxi}}$ appear to increase R_j . Comparing junction A with junction B, which were both produced with the same $P_{\text{pl-oxi}}$, the R_j becomes approximately 8 times larger for junction B with the increase in $t_{\text{pl-oxi}}$ (Table 2). Additionally, this change in R_j could not have been due to a change in the junction area, A_j , as the area would need to be approximately 8 times smaller for junction B in order to be the sole cause of the R_j increase. However, as the junction area is defined by hand as described in Section 2.1, such a large decrease in A_j would not be possible. Consequently, the increase in R_j seen for junction B must

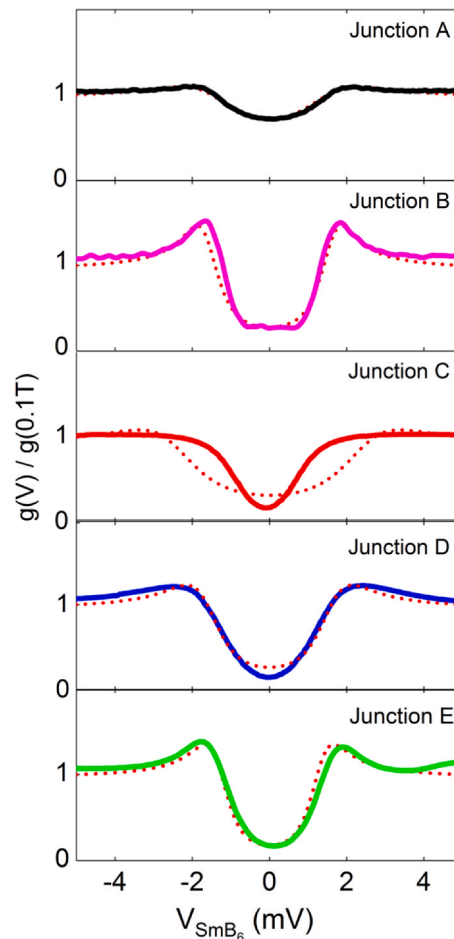


Fig. 8. Background-normalized conductance spectra of $\text{SmB}_6/\text{SmB}_6\text{-Oxi}/\text{Pb}$ junctions processed with plasma cleaning and the best fits to the BTK model. $g(V)$ curves of $\text{SmB}_6/\text{SmB}_6\text{-Oxi}/\text{Pb}$ junctions at zero field divided by $g(V)$ at finite field ($H = 0.1$ T) (solid lines) and the best fits to the BTK model [12] (dotted lines).

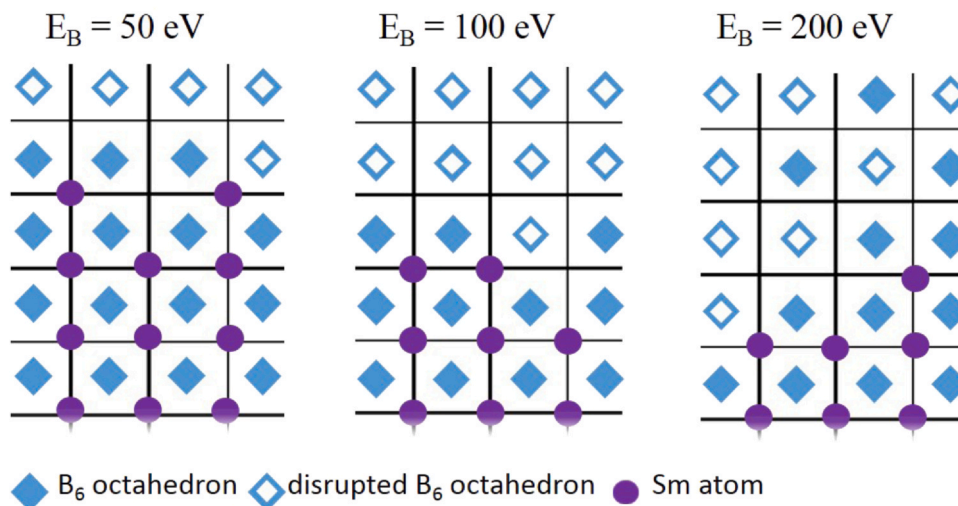


Fig. 9. Possible schematic of the SmB_6 crystal lattice after ion beam etching (side view). When the ion beam energy, $E_B = 50$ or 100 eV, both the sputter yield and the depth from the surface an incoming ion can penetrate would be significantly smaller than for $E_B = 200$ eV [22]. When $E_B = 50$ eV, the depth of the disrupted boron octahedra may be so thin that the barrier formed may have a few small discontinuities within the junction area. When $E_B = 100$ eV, a few layers of disrupted boron octahedra may remain after etching, which once oxidized may form a high quality continuous barrier. Additionally, at $E_B = 200$ eV the layers left behind as surface layers are removed may consist of a mixture of disrupted and intact boron octahedra. This may result in a barrier containing a mixture of B_6O and B_2O_3 .

have resulted from the increase in $t_{\text{pl-oxi}}$. Therefore, the improvement in the junction characteristics (higher Z and lower R_j) seen for junctions C, D, and E most likely resulted from the increase in $P_{\text{pl-oxi}}$ rather than $t_{\text{pl-oxi}}$.

B_6O may be forming on the SmB_6 crystals oxidized with lower $P_{\text{pl-oxi}}$ due to the initial configuration of the boron atoms, which is more similar to the configuration of boron in B_6O compared to B_2O_3 . Furthermore, studies utilizing XPS observe the formation of B_6O on boron terminated SmB_6 surfaces exposed to residual gases in a vacuum [26,27]. Conversely, higher $P_{\text{pl-oxi}}$ may be needed to form B_2O_3 in order to disrupt the B_6 octahedra due to the rigid, covalently bonded nature of the boron bonds [26]. Therefore, the $P_{\text{pl-oxi}}$ and how quickly its power dissipates as it penetrates the sample would limit the thickness of B_2O_3 formed. However, as B_6O has been observed to form on SmB_6 at room temperature [26,27], the thickness of B_6O is not likely subjected to this same constraint in $P_{\text{pl-oxi}}$. Although suboxide formation would be less dominant at the higher $P_{\text{pl-oxi}}$, traces of suboxides may still be problematic at lower $P_{\text{pl-oxi}}$, as supported by the non-negligible Γ .

For the junctions fabricated on the ion beam etched surfaces, the junction prepared with the highest $E_B = 200$ eV showed properties likely due to suboxide formation. As the plasma cleaned and ion beam etched junctions were processed in separate chambers, no direct comparison can be made between the powers used during the oxidation processes. However, as the 200 eV junction displays properties likely due to suboxide formation, the $P_{\text{pl-oxi}}$, which is ~ 1 W for the ion beam etched junctions, may not be large enough to disrupt the B_6 octahedron and form B_2O_3 .

The question then remains as to why the junctions processed with lower E_B , have characteristics expected of a B_2O_3 tunnel barrier. As the power of oxidation remained constant for all junctions, the change in junction characteristics must have resulted from chemical changes made to the crystal surface during the ion beam etching process. Consistent with what was described previously, at low $P_{\text{pl-oxi}}$, B_2O_3 would be more likely to form on the disrupted octahedra, i.e., B_5 , B_4 , B_3 , etc, and B_6O would more naturally form on boron octahedra left intact [26].

For the $E_B = 50$ eV case, the sputter yield will be the lowest and the incoming ions are likely to only etch atoms from the surface layer [28]. This may leave a very thin layer of disrupted octahedra after the etching process. However, if this layer is too thin, it may be discontinuous with a few spare B_6 octahedra left intact. Following

this logic, once oxidized, the barrier may consist primarily of B_2O_3 with sparse B_6O impurities, resulting in a limited number of micro shorts along the interface. If the number of micro shorts is small, Z may still be large as shown in Table 2. Additionally, this picture is consistent with the conductance spectra shown in Fig. 5(b), which may be primarily due to tunneling but with a small contribution from the point contacts as the conductance spectra exhibited sharp coherence peaks but no spin exciton features are seen.

For the junction processed with $E_B = 200$ eV, the sputter yield will be the highest and layers of the material will be removed at the fastest rate [28]. Additionally, at higher E_B , both the average distance from the surface an incoming ion can penetrate and the uncertainty in the ions' penetration depth increase [28]. Therefore, as a new layer is removed from the surface, it may leave behind a mixture of disrupted and intact octahedra as shown in Fig. 9. Once oxidized, this would result in a thick barrier comprised of both B_6O and B_2O_3 . For the 100 eV case, the incoming ions may penetrate further into the sample than the 50 eV case yet etch from a shallower depth than the 200 eV case [28]. It is possible for approximately two to three layers of the disrupted octahedra to remain after etching (Fig. 9) as this thickness would correspond to the thickness of the barrier discussed in Section 2.4.

Due to the weak signal in second harmonic measurements, even scarce impurities or suboxides can be detrimental to the resolution of features. Depositing an oxide barrier directly may improve junction quality but preventing interaction with the nearby oxide is a concern. For example, previous PTS studies observe the diffusion of Al into SmB_6 [9] and XPS studies show that depositing MgO on CoFeB results in a layer of boron oxides [29]. To prevent interaction with the oxide barrier, reducing the temperature of deposition [9], or taking advantage of the protection offered by Sm-terminated surfaces [30–32] may improve results as they help protect the lower layers from reconstruction [30] and do not oxidize as easily as the B-terminated surfaces [27]. Alternatively, depositing hexagonal boron nitride [33] as the insulating barrier may eliminate accidental oxidation, possibility resulting in higher quality junctions.

5. Conclusion and outlook

Planar tunnel junctions were prepared on SmB_6 single crystals using Pb counter-electrodes and the SmB_6 surface was oxidized

using plasma oxidation. The influence of two different surface cleaning methods, ion beam etching and plasma cleaning, on the junction quality was investigated and both methods were able to produce the expected SmB_6 features. Simulations based on the Blonder-Tinkham-Klapwijk model revealed several junctions with lower barrier strength and the data showed that these same junctions typically had higher resistances; an effect contradictory to the resistance and barrier strength relation the BTK theory proposes. The formation of suboxides may be able to explain the unusual results as electrons tunneling through different oxide layers would undergo a more complicated diffusion/tunneling process. This suboxide formation seems to be more dominant at higher ion beam energies as well as lower plasma oxidation powers. In order for the second harmonic data to reveal clear features, the junction quality should still be improved. By depositing an alternative material such hexagonal boron nitride, problematic suboxide formation or diffusion into SmB_6 may be avoided.

CRedit authorship contribution statement

WKP designed the experiment and JS performed the experiment. Both WKP and JS analyzed the data. JS drafted the manuscript and WKP revised it.

Declaration of Competing Interest

The authors declare that they have no known competing financial interests or personal relationships that could have appeared to influence the work reported in this paper.

Acknowledgments

We acknowledge L. H. Greene, K. Shrestha, and S. Zhang for helpful discussions. This work was supported by the US National Science Foundation (NSF), Division of Materials Research (DMR), under Award No. NSF/DMR-1704712. A portion of this work was performed at the National High Magnetic Field Laboratory, which is supported by the NSF Cooperative Agreement No. NSF/DMR-1644779 and the State of Florida. The high quality SmB_6 crystals used in this work were provided by Z. Fisk at the University of California-Irvine and T. M. McQueen at the Johns Hopkins University.

References

- [1] G. Aeppli, Z. Fisk, Kondo Insulators, *Comments Condens. Matter Phys.* 16, 1992, 155.
- [2] P.S. Riseborough, Heavy fermion semiconductors, *Adv. Phys.* 49 (2000) 257–320.
- [3] M. Dzero, K. Sun, V. Galitski, P. Coleman, Topological Kondo insulators, *Phys. Rev. Lett.* 104 (2010) 106408.
- [4] M. Dzero, J. Xia, V. Galitski, P. Coleman, Topological Kondo insulators, *Annu. Rev. Condens. Matter Phys.* 7 (2016) 249–280.
- [5] W.T. Fuhrman, J. Leiner, P. Nikolic, G.E. Granroth, M.B. Stone, M.D. Lumsden, L. DeBeer-Schmitt, P.A. Alekseev, J.M. Mignot, S.M. Koohpayeh, P. Cottingham, W.A. Phelan, L. Schoop, T.M. McQueen, C. Broholm, Interaction driven subgap spin exciton in the Kondo insulator SmB_6 , *Phys. Rev. Lett.* 114 (2015) 036401.
- [6] P.S. Riseborough, Collapse of the coherence gap in Kondo semiconductors, *Phys. Rev. B* 68 (2003) 235213.
- [7] G.A. Kapilevich, P.S. Riseborough, A.X. Gray, M. Gulacsi, T. Durakiewicz, J.L. Smith, Incomplete protection of the surface Weyl cones of the Kondo insulator SmB_6 : spin exciton scattering, *Phys. Rev. B* 92 (2015) 085133.
- [8] W.K. Park, L. Sun, A. Noddings, D.-J. Kim, Z. Fisk, L.H. Greene, Topological surface states interacting with bulk excitations in the Kondo insulator SmB_6 revealed via planar tunneling spectroscopy, *Proc. Natl. Acad. Sci. USA* 113 (2016) 6599–6604.
- [9] L. Sun, D.J. Kim, Z. Fisk, W.K. Park, Planar tunneling spectroscopy of the topological Kondo insulator SmB_6 , *Phys. Rev. B* 95 (2017) 195129.
- [10] W.K. Park, J.A. Sittler, L.H. Greene, W.T. Fuhrman, J.R. Chamorro, S.M. Koohpayeh, W.A. Phelan, T.M. McQueen, Topological nature of the Kondo insulator SmB_6 and its sensitiveness to Sm vacancy, *Phys. Rev. B* 103 (2021) 155125.
- [11] W.L. McMillan, J.M. Rowell, Lead phonon spectrum calculated from superconducting density of states, *Phys. Rev. Lett.* 14 (1965) 108–112.
- [12] E.L. Wolf, *Principles of Electron Tunneling Spectroscopy*, Oxford University Press, Inc., New York, 1985.
- [13] G.E. Blonder, M. Tinkham, T.M. Klapwijk, Transition from metallic to tunneling regimes in superconducting microconstrictions: excess current, charge imbalance, and supercurrent conversion, *Phys. Rev. B* 25 (1982) 4515–4532.
- [14] B. Amsler, Z. Fisk, J.L. Sarrao, S. von Molnar, M.W. Meisel, F. Sharifi, Electron-tunneling studies of the hexaboride materials SmB_6 , EuB_6 , CeB_6 , and SrB_6 , *Phys. Rev. B* 57 (1998) 8747–8750.
- [15] S. Rössler, T.H. Jang, D.J. Kim, L.H. Tjeng, Z. Fisk, F. Steglich, S. Wirth, Hybridization gap and Fano resonance in SmB_6 , *Proc. Natl. Acad. Sci. USA* 111 (2014) 4798–4802.
- [16] W. Ruan, C. Ye, M.H. Guo, F. Chen, X.H. Chen, G.M. Zhang, Y.Y. Wang, Emergence of a coherent in-gap state in the SmB_6 Kondo insulator revealed by scanning tunneling spectroscopy, *Phys. Rev. Lett.* 112 (2014) 136401.
- [17] M.M. Yee, Y. He, A. Soumyanarayanan, D.-J. Kim, Z. Fisk, J.E. Hoffman, Imaging the Kondo insulating gap on SmB_6 , *arXiv* 1308 (2013) 1085.
- [18] X.H. Zhang, N.P. Butch, P. Syers, S. Ziemak, R.L. Greene, J. Paglione, Hybridization, inter-ion correlation, and surface states in the Kondo insulator SmB_6 , *Phys. Rev. X* 3 (2013) 011011.
- [19] D.J. Kim, J. Xia, Z. Fisk, Topological surface state in the Kondo insulator samarium hexaboride, *Nat. Mater.* 13 (2014) 466–470.
- [20] W.A. Phelan, S.M. Koohpayeh, P. Cottingham, J.A. Tutmaher, J.C. Leiner, M.D. Lumsden, C.M. Lavelle, X.P. Wang, C. Hoffmann, M.A. Siegler, N. Haldolaarachchige, D.P. Young, T.M. McQueen, On the chemistry and physical properties of flux and floating zone grown SmB_6 single crystals, *Sci. Rep.* 6 (2016) 20860.
- [21] National Physical Laboratory, *Densities and Energies of Sublimation*, 2005, (https://www.npl.co.uk/getattachment/research/mass-spectrometry/Secondary-ion/Sputter-yieldvalues/energy_density_sublim.pdf.aspx?lang=en-GB).
- [22] W.F. Brinkman, R.C. Dynes, J.M. Rowell, Tunneling conductance of asymmetrical barriers, *J. Appl. Phys.* 41 (1970) 1915–1921.
- [23] D. Li, W.Y. Ching, Electronic structures and optical properties of low- and high-pressure phases of crystalline B_2O_3 , *Phys. Rev. B* 54 (1996) 13616–13622.
- [24] W.E. Moddeman, A.R. Burke, W.C. Bowling, D.S. Foose, Surface oxides of boron and B_{12}O_2 as determined by XPS, *Surf. Interface Anal.* 14 (1989) 224–232.
- [25] C.W. Ong, H. Huang, H. Hom, B. Zheng, R.W.M. Kwok, Y.Y. Hui, W.M. Lau, X-ray photoemission spectroscopy of nonmetallic materials: electronic structures of boron and B_2O_3 , *Appl. Phys. Lett.* 95 (2004) 3527–3534.
- [26] N. Heming, U. Treske, M. Knupfer, B. Buchner, D.S. Inosov, N.Y. Shitsevalova, V.B. Filipov, S. Krause, A. Koitzsch, Surface properties of SmB_6 from X-ray photoelectron spectroscopy, *Phys. Rev. B* 90 (2014) 195128.
- [27] P. Lutz, M. Thees, T.R.F. Peixoto, B.Y. Kang, B.K. Cho, C.H. Min, F. Reinert, Valence characterisation of the subsurface region in SmB_6 , *Philos. Mag.* 96 (2016) 3307–3321.
- [28] S. Cabrini, S. Kawata, *Nanofabrication Handbook*, 1st ed., CRC Press, 2012.
- [29] T.N. Tran, T.N. Lam, C.Y. Yang, W.C. Lin, P.W. Chen, Y.C. Tseng, Superparamagnetic ground state of CoFeB/MgO magnetic tunnel junction with dual-barrier, *Appl. Surf. Sci.* 457 (2018) 529–535.
- [30] V.B. Zabolotnyy, K. Fursich, R.J. Green, P. Lutz, K. Treiber, C.H. Min, A.V. Dukhnenko, N.Y. Shitsevalova, V.B. Filipov, B.Y. Kang, B.K. Cho, R. Sutarto, F.Z. He, F. Reinert, D.S. Inosov, V. Hinkov, Chemical and valence reconstruction at the surface of SmB_6 revealed by means of resonant soft X-ray reflectometry, *Phys. Rev. B* 97 (2018) 205416.
- [31] M. Futamoto, U. Kawabe, Field-ion microscopy of rare-earth hexaborides, *Surf. Sci.* 93 (1980) L117–L123.
- [32] M. Aono, R. Nishitani, C. Oshima, T. Tanaka, E. Bannai, S. Kawai, LaB_6 and SmB_6 (001) surfaces studied by angle-resolved XPS, LEED, and ISS, *Surf. Sci.* 86 (1979) 631–637.
- [33] C. Elias, P. Valvin, T. Pelini, A. Summerfield, C.J. Mellor, T.S. Cheng, L. Eaves, C.T. Foxon, P.H. Beton, S.V. Novikov, B. Gil, G. Cassabois, Direct band-gap cross-over in epitaxial monolayer boron nitride, *Nat. Commun.* 10 (2019) 2639.